Composites Science and Technology 84 (2013) 1–7

Contents lists available at SciVerse ScienceDirect

Composites Science and Technology

journal homepage: www.elsevier.com/locate/compscitech

Polypropylene/graphene nanosheet nanocomposites by *in situ* polymerization: Synthesis, characterization and fundamental properties

Marcéo A. Milani [a], Darío González [b], Raúl Quijada [b], Nara R.S. Basso [c], Maria L. Cerrada [d], Denise S. Azambuja [a], Griselda B. Galland [a,*]

[a] Instituto de Química, Universidade Federal do Rio Grande do Sul, Av. Bento Gonçalves 9500, 91501-970 Porto Alegre, Brazil
[b] Departamento de Ingeniería Química y Biotecnología, Facultad de Ciencias Físicas y Matemáticas, Universidad de Chile, Casilla 2777, Santiago, Chile
[c] Faculdade de Química, Pontifícia Universidade Católica do Rio Grande do Sul-Brasil, Av. Ipiranga 6681, 90619-900 Porto Alegre, Brazil
[d] Instituto de Ciencia y Tecnología de Polímeros (ICTP-CSIC), Juan de la Cierva 3, 28006 Madrid, Spain

ARTICLE INFO

Article history:
Received 3 October 2012
Received in revised form 28 April 2013
Accepted 1 May 2013
Available online 15 May 2013

Keywords:
Graphene nanosheets
A. Nano composites
B. Mechanical properties
B. Electrical properties
D. Dynamical mechanical thermal properties (DMTA)

ABSTRACT

This study investigates the synthesis, characterization and properties of isotactic polypropylene/graphene nanosheet nanocomposites (iPP/GNS). These nanocomposites were prepared by *in situ* polymerization using the metallocene complex *rac*-$Me_2Si(Ind)_2ZrCl_2$ and methylaluminoxane (MAO) as cocatalyst. Homogeneous graphene nanosheet dispersions within the polymeric matrix were observed by TEM and XRD. The molecular characteristics of iPP, such as molecular weight, polydispersity and tacticity, were not affected by the presence of nanoparticles. The thermal properties investigated by DSC and TGA showed that graphene nanosheets significantly improved the matrix, increasing the crystallization and the degradation temperatures. From a mechanical perspective, there was an excellent balance between a significant increase in Young's modulus and a slight reduction in the elongation at break. The reinforcing effect of graphene incorporation was confirmed by the increase of the storage modulus with nanosheet content. An enhancement of dimensional stability was also detected, and deformability was significantly smaller in the nanocomposites than in the homopolymer. Impedance measurements showed that the electrical conductivity increased by a factor of 10^8 compared to that of neat iPP.

1. Introduction

Polymeric nanocomposites are materials composed of organic or inorganic fillers and polymers, where at least one dimension of the dispersed particles is in the nanometer range [1]. Polypropylene, when reinforced with micro- and nanofillers, shows high stiffness and strength, and it is commonly used in the automotive and aerospace industries [2]. Many nanocomposites have been prepared by mixing the nanofiller with the polymer in its molten state [3]. In this procedure, the nanofiller particles tend to agglomerate rather than disperse, which is a disadvantage. The *in situ* polymerization approach, i.e., the polymerization of monomers in the presence of nanofiller, shows promising results for the improvement of nanofiller dispersion in the polymeric matrix [4,5]. A good dispersion is of critical importance for the final properties of the nanocomposite.

Industrial interest in graphite as filler has increased enormously. In fact, graphene is stronger than steel and conducts electricity, at room temperature, better than any other material known to mankind [6,7]. There is a wide variety of possible graphene applications, including the creation of new materials and the production of innovative electronic devices [8]. Graphite naturally occurs in the form of flakes or powders of various particle size [9]. However, the preparation of nanocomposites by direct intercalation is difficult, requiring the chemical or physical modification of graphite. Changes in graphite structure are usually made by intercalation with chemical species to form graphite intercalated compounds (GICs), which expand at high temperatures, producing expanded graphite (EG) [10–12]. Finally, graphene nanosheets (GNSs) can be prepared by dispersing EG in an ultrasound bath. Because of the excellent electrical, mechanical and thermal properties of graphene, the resulting nanocomposites are electrical conductors with improved heat resistance and stiffness [13–15]. In the literature, some papers report the preparation of isotactic polypropylene (iPP) nanocomposites with graphite or graphite oxide by molten state blending [16–18], solid state shear pulverization [19] and solution processes [20]. However, the *in situ* polymerization of propylene with graphite or graphite-derived materials has been studied rarely until now. Very recently, Dong et al. [21,22] described the synthesis of PP nanocomposites using graphite oxide delaminated with a Grignard reagent supported

* Corresponding author. Tel.: +55 5133087317; fax: +55 5133087304.
E-mail address: griselda.barrera@ufrgs.br (G.B. Galland).

0266-3538/$ - see front matter © 2013 Elsevier Ltd. All rights reserved.
http://dx.doi.org/10.1016/j.compscitech.2013.05.001

on a $TiCl_4$ catalyst. Those authors claim to have observed unique electrical conductivity at a very low percolation threshold. While we were concluding our work on this manuscript, Shevchenko et al. [23] published a paper concerning the use of *in situ* polymerization to prepare PP/graphene nanoplatelets with good exfoliation. However, their catalytic activities were much lower than ours; they used higher PP pressures and Al/Zr ratios than in our study and they did not investigate the thermal stability, molecular weight and dynamic-mechanical properties of their composites. In a preliminary study, our research group [24] studied two types of graphene nanosheets (GNSs) and metallocene catalysts to synthesize isotactic polypropylene–graphene (iPP/GNS) nanocomposites with good molecular weight, crystallinity and tacticity. However, we did not analyze the properties of those materials. The present study includes a detailed examination of the properties of iPP/GNS nanocomposites obtained through *in situ* polymerization.

2. Experimental

2.1. Materials

All manipulations were performed using standard Schlenk tube techniques under deoxygenated dried argon. Expanded graphite (Micrograf HC11) was provided by Nacional de Grafite Ltda. (Brazil). Toluene was distilled with metallic sodium and benzophenone. Methylaluminoxane, MAO, (Witco, 10 wt.% Al solution in toluene) and the metallocene catalyst *rac*-$Me_2Si(Ind)_2ZrCl_2$ (Chemtura) were used as received.

2.2. Preparation of graphene nanosheets

The preparation of graphene nanosheets from graphite flake and the characterization of the nanosheets were described in our previous papers [9,24]. The expanded graphite was suspended in ethanol at a concentration of 70%, and the suspension was placed in an ultrasound bath for 8 h. Then, the solution was filtered, and the graphene nanosheets were dried at 120 °C for 48 h.

2.3. Polymerization reactions

Polymerization reactions were performed at a controlled temperature (40 °C) using a 1000 mL Büchi glass reactor equipped with mechanical stirring. First, toluene as a solvent, MAO (Al/Zr = 1000) as a cocatalyst and graphene nanosheets in amounts from 0.5 to 20 wt.% were added to the reactor. A wide range of GNS values were chosen to study their influence on nanocomposites properties. Then, propylene was fed into the reactor at atmospheric pressure, and the catalyst *rac*-$Me_2Si(Ind)_2ZrCl_2$ (5×10^{-6} mol) was added. The reactor was fed continuously with propylene to maintain a constant pressure of 2.8 bar during 0.5 h. The polymerizations were terminated by the addition of 5 vol.% HCl in ethanol. The polymers were washed with water and dried to a constant weight. Each polymerization was repeated until a maximum deviation of 10% in catalytic activity was obtained in three reactions, and these values were used to calculate the average.

2.4. Characterization and properties of homopolymers and nanocomposites

Calorimetric analyses were carried out in a TA Instruments Q20 calorimeter at a heating rate of 10 °C/min^{-1} from 25 to 160 °C. Thermogravimetric analysis (TGA) was performed on a SDT Q600 thermal analyzer Q20 (TA Instruments) at a scanning rate of 20 °C/min from 25 to 1000 °C. X-ray diffraction (XRD) measurements were obtained on a diffractometer Rigaku DMAX 2200 equipped with a Cu tube and a secondary monochromator. The goniometer was a Siemens D500, and the detector was a scintillator (NaI and Tl). The samples were analyzed in powder form at room temperature. Molecular weights were estimated using a Waters Alliance GPC 2000 instrument at 135 °C. The polymeric microstructure was determined by ^{13}C-NMR at 130 °C in a Varian Inova 300 operating at 75 MHz. Sample solutions of polymers in *o*-dichlorobenzene and benzene-d_6 (20% v/v) were prepared in 5 mm sample tubes. Scanning Electronic Microscopy (SEM) analyses were carried out using a Phillips microscope, model XL30, operating at 20 kV. Samples were deposited on aluminum stubs and coated with gold. Transmission Electronic Microscopy (TEM) images were obtained using a JEOL 1200 ExII transmission electron microscope operated at 100 kV. Samples were prepared by depositing drops of solution on a grid or by cutting ultrathin films (~70 nm) under cryogenic conditions with a Leica Ultracut UCT microtome at −80 °C and placing pieces on a grid. Tensile properties were evaluated with an HP model D-500 dynamometer. Dumbbell-shaped samples with an effective thickness of 1 mm, a length of 80 mm and a width of 12 mm were cut from compression-molded sheets. Samples were tested at a rate of 50 mm/min at room temperature. Viscoelastic properties were measured in a Polymer Laboratories MK II dynamic mechanical thermal analyzer working in tensile mode. The complex modulus and the loss tangent for each sample were determined at 1, 3, 10 and 30 Hz over a temperature range from −140 to 150 °C, at a heating rate of 1.5 °C/min. These measurements were performed on iPP/graphene nanosheet nanocomposite films (approximately 450 μm) processed by compression molding in a Collin press between hot plates at 200 °C at a pressure of 25 bar for 5 min. A fast quench in cold water was applied after melting in the press. The electrical conductivity of the nanocomposites was obtained by impedance measurements, as described in the literature [25]. These impedance experiments were performed using an AUTOLAB PGSTAT 30/FRA 2 in the 1 MHz to 100 mHz frequency range with a sinusoidal voltage amplitude of 10 mV. Thus, the electrical conductivity of the polymeric film could be calculated by the following equation: $\sigma = 1/\mathrm{Rb}\ (d/S)$, where σ is the electrical conductivity, d is the film thickness, S is the area of electrodes in contact with the polymeric film and Rb is the bulk resistance.

3. Results and discussion

3.1. In situ polymerization reactions

The polymerization reactions were performed using the metallocene catalyst *rac*-$Me_2Si(Ind)_2ZrCl_2$ and methylaluminoxane (MAO) as a cocatalyst. The graphene nanosheets (GNSs) were stirred for 15 min with MAO to eliminate impurities or to block functional groups that could remain from the graphite oxidation. Table 1 lists the series of polymerization reactions performed with different amounts of GNS and the results for the catalytic activity, molecular weight, polydispersity and tacticity. The percentages of graphene nanosheets in nanocomposites were determined using reaction yields and TGA residues, and both approaches indicated good sample homogeneity. The catalytic activity tended to decrease with the increasing graphene amounts, showing that some remaining active polar functional groups deactivated the catalyst. Nevertheless, the amount of MAO was kept constant, even in polymerizations with high GNS contents, because the amount of nanocomposite product was high enough to study the properties of the polymers. The molecular weight, polydispersity and tacticity estimated for the nanocomposites were compared with those found in the neat polymer (iPP) and did not differ significantly from the iPP.

Table 1
Results of the *in situ* polymerization reactions for iPP/GNS nanocomposites.

Sample	GNS- yield[a] (wt.%)	GNS- TGA[b] (wt.%)	Polymer Yield (g)	Activity(kgPP/ n_{Zr}.bar.h.)	M_w (g/ mol)	M_w/M_n	Tacticity *m* (mol%)	T_m (°C)	T_c (°C)	X_c (%)	T_{onset} (°C)	T_{max} (°C)	σ_{ac} (S cm^{-1})
1	–	–	68.7	9814	74,641	1.4	96.1	145	109	45	443	466	1.5×10^{-13}
2	0.5	0.5	64.8	9257	n.d	n.d	96.4	146	113	41	451	475	n.d.
3	1.1	0.9	60.4	8629	75,262	1.4	96.7	146	114	46	452	476	4.6×10^{-13}
4	2.5	2	54.3	7757	75,963	1.4	95.4	147	115	44	452	477	5.4×10^{-12}
5	3.4	2.8	51.8	7400	n.d	n.d	n.d	147	116	42	453	477	n.d.
6	4.8	4.8	41.3	5900	n.d	n.d	97.1	147	117	40	454	479	2.7×10^{-11}
7	8.2	7.6	36.7	5243	n.d	n.d	n.d	147	119	41	460	483	1.2×10^{-10}
8	13.2	12.3	26.4	3771	75,705	1.5	96.4	147	119	40	466	487	4.4×10^{-8}
9	15.3	13.6	22.8	3257	n.d	n.d	n.d	147	120	41	467	489	n.d.
10	20.2	17.4	20.9	2986	n.d	n.d	n.d	147	121	40	470	491	3.4×10^{-5}

Reaction conditions: P = 2.8 bar, T = 40 °C, [Zr] = 5 μmol, Al/Zr = 1000, t = 30 min, V_{tol} = 400 mL.
[a] GNS percentage calculated from the polymer yield.
[b] GNS percentage obtained by TGA residue.

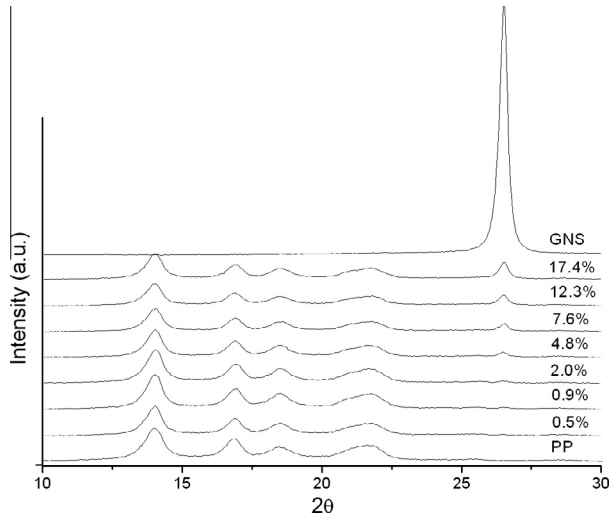

Fig. 1. X-ray diffraction data for neat iPP, GNS and iPP/GNS nanocomposites.

3.2. X-ray diffraction (XRD)

Fig. 1 shows the X-ray diffraction data for neat iPP, the graphene nanosheets and the iPP/GNS nanocomposites. The GNS diffractogram has a strong peak at $2\theta \approx 26.5°$ that is characteristic of the spacing between graphene units in the 002 plane. The neat iPP profile is related to its α monoclinic modification, exhibiting the five main diffraction peaks of this crystalline lattice corresponding to the (110), (040), (130), (111) and (130, 041) planes, in order of increasing angles. For iPP, none of the peaks is located near 26.5°. In the iPP/GNS nanocomposites, the characteristic GNS peak appears only at 4.8 wt.% and higher levels of GNS. This indicates complete exfoliation and a good dispersion of the graphene nanosheets in the nanocomposites with low GNS contents. For composites with higher GNS contents, the graphite peak indicates that the GNS is dispersed in the polymer but not completely exfoliated.

3.3. Scanning Electronic Microcopy (SEM)

Fig. 2 shows the SEM images taken at the fracture surfaces after deformation measurements for neat iPP (a) and its nanocomposites (b–f), and the differences in morphology are clearly evident. Pristine iPP exhibits a smooth surface, while nanocomposites show layered structures because GNS is well covered by the polymeric matrix.

3.4. Transmission Electronic Microscopy (TEM)

Fig. 3 shows TEM images of a iPP/GNS nanocomposite that contains 12.3 wt.% GNS. The graphene nanosheets (black lines) are visible in the micrographs of samples prepared by depositing solution drops (Fig. 3a and b) or ultrathin films (Fig. 3c and d). Graphene nanosheets are less visible in the nanocomposites with low GNS levels, most likely due to their low concentrations as well as their exfoliation, as indicated by the absence of characteristic graphene spacing in the XRD profiles. The graphene nanosheets dispersed in nanocomposites containing 12.3 wt.% GNS, depicted in Fig. 3, have an average thickness of 7.9 nm, which corresponds to 18 graphene units per nanosheet.

3.5. Thermal properties

Table 1 shows the thermal properties of iPP and its nanocomposites. The values of the melting temperature and the degree of crystallinity do not change significantly with the amount of GNS. In contrast, the considerable increase (more than 10 °C) in the crystallization temperature indicates that the graphene nanosheets are functioning as nucleating agents in these nanocomposites. High crystallization temperatures are very interesting because they allow a reduction in the processing cycle, which consequently increases the production rate [16]. Increasing the amount of GNS in these nanocomposites also raises the initial degradation temperature (T_{onset}) and the maximum mass loss temperature (T_{max}) relative to the temperatures for neat iPP. An enhancement of approximately 10 °C in both temperatures is observed using only 2 wt.% GNS, while an increase greater than 20 °C is observed above 12.3 wt.% GNS (see Table 1). These features are strong indications that graphite can function as a flame retardant, significantly improving the thermal stability of isotactic polypropylene. Fang [20], coating graphene with PP latex and then melt-mixing in a PP matrix, and Torkelson [19], using a solid-state shear pulverization method, also obtained a significant increase in the initial and maximum mass loss temperatures. However, the degradation temperatures obtained in our study are significantly greater than those reported by those authors. This difference can be attributed to the preparation of the iPP using a metallocene catalyst that produces polyolefins with very narrow polydispersity ($M_w/M_n < 2$), as reported in Table 1. All of the other previously published studies on these types of nanocomposites involved iPP obtained with Ziegler–Natta catalysts, which produce broad molecular weight dispersions. The shorter chains present in those materials start to degrade at lower temperatures than longer chains. Using metallocene catalysts, homogeneous materials can be synthesized and used as accurate models in comprehensive studies of the properties affording tunable behavior because of the versatility of the materials.

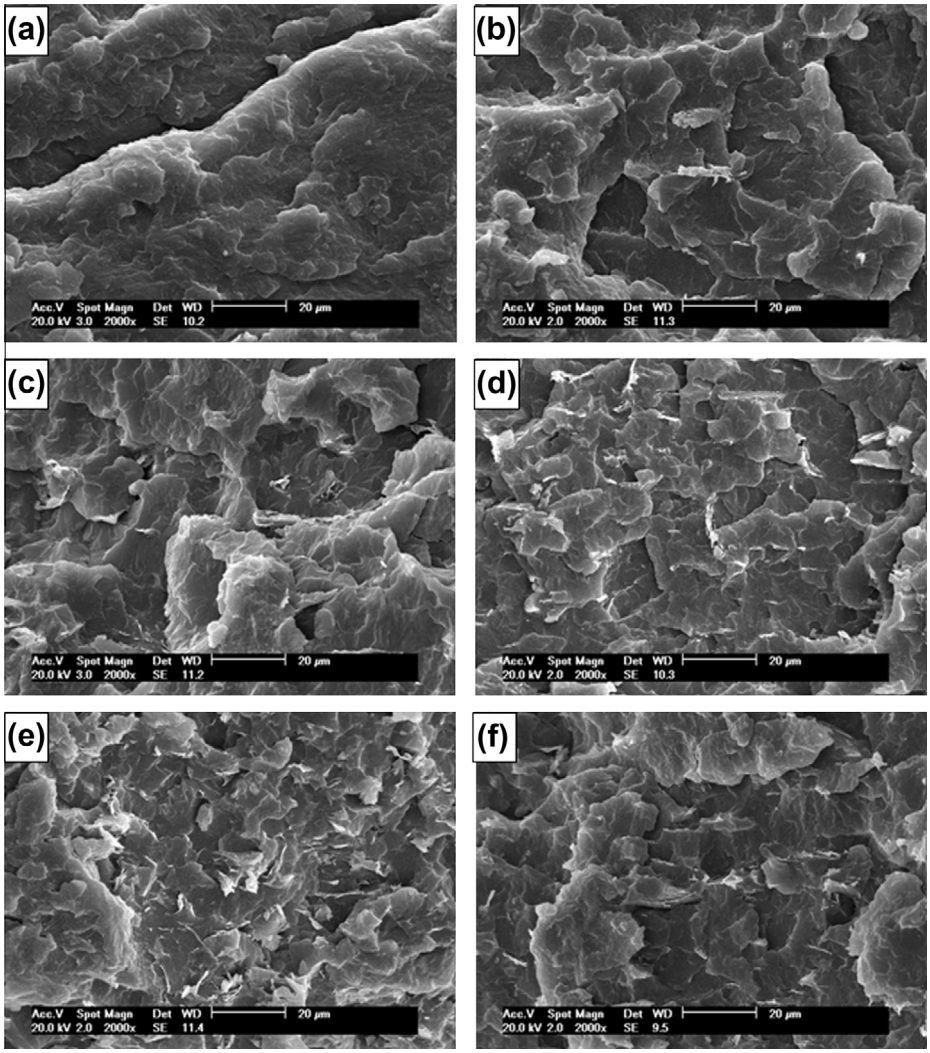

Fig. 2. SEM images (20 μm) of the tensile broken sections of: (a) neat iPP, (b) iPP/GNS 0.9%, (c) iPP/GNS 2.0%, (d) iPP/GNS 4.8%, (e) iPP/GNS 7.6% and (f) iPP/GNS 12.3%.

3.6. Mechanical properties

Fig. 4 clearly shows the considerable change in Young's modulus as GNS is incorporated in the iPP polymeric matrix. A significant increase is observed, from 1280 ± 42 MPa in neat iPP to approximately 1920 ± 63 MPa (approximately 50% greater rigidity) in the iPP/GNS nanocomposite with the highest GNS content (17.4 wt.%).

Fig. 5a shows that GNS incorporation also leads to an increase in the tensile strength values to a maximum of 2.6 MPa for the iPP/GNS nanocomposite with 4.8% GNS, i.e., an increase of approximately 25% compared with neat iPP. The presence of graphene agglomerates above 4.8 wt.% GNS, as shown by the XRD measurements, does not contribute to a further increase in tensile strength, although the lowest tensile value in nanocomposites with high GNS loading is similar to that exhibited by the pristine iPP. Moreover, the small decrease in the elongation at break (Fig. 5b) for the nanocomposites compared to the iPP matrix is a remarkable feature. This reduction is only approximately 12% for nanocomposites containing less than 4.8 wt.% GNS, and it increases to approximately 30% for higher GNS loadings. The formation of graphene agglomerates seems to play a significant role.

Torkelson [19], using solid-state shear pulverization, and Fang [20], using melt blending, observed increases in Young's modulus up to 1830 and 1760 MPa at graphite loadings of 2.7 and 1 wt.%, respectively, and significant decreases at higher graphene contents.

The results observed previously by Torkelson [19] and Fang [20] differ from our results for nanocomposites prepared by *in situ* polymerization, where the modulus continuously increased with GNS content. This is a primary and important practical difference between these *in situ* nanocomposites and nanocomposites prepared using other methods. The degree of dispersion and the agglomerate sizes are sufficient to produce stiffer nanocomposites at a graphene levels as high as 17.4 wt.%. Some researchers have reported a significant decrease for the elongation at break. The iPPs prepared using ZN catalysts have much broader polydispersity than metallocene iPP and consequently their elongation at break is also much higher. The polymeric chains with low molecular weights can act as a plasticizer and the reduction of elongation at break in those ZN nanocomposites becomes much significant.

3.7. Dynamic mechanical properties

Fig. 6 shows the variation of the storage modulus and the loss tangent for different specimens. The upper plot shows an increase in the storage modulus with increasing graphene nanosheet content in the nanocomposites, which is consistent with the trend obtained from uniaxial deformation. Therefore, the increase in rigidity can be attributed to the reinforcing effect of graphene, as crystalline graphene is one of the stiffest materials in nature. However, this improvement of rigidity with GNS content is more

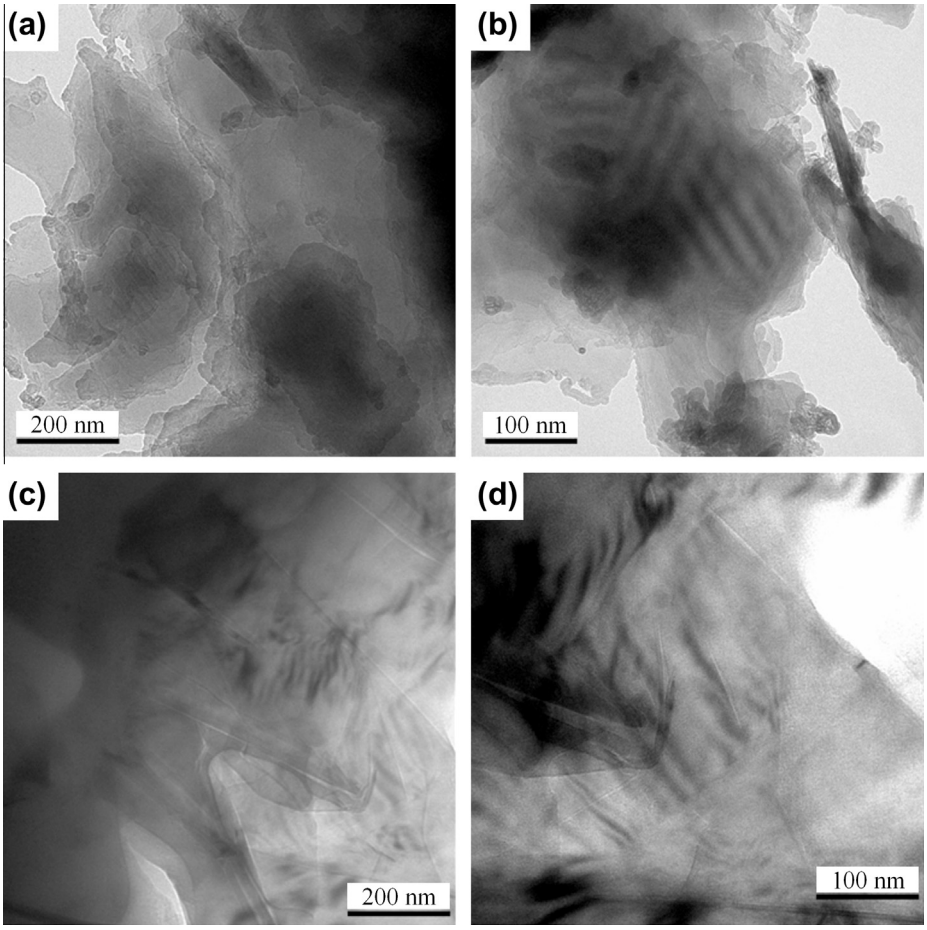

Fig. 3. TEM images of an iPP/GNS nanocomposite with 12.3 wt.% GNS prepared by solution drops (a and b) or ultrathin films (c and d).

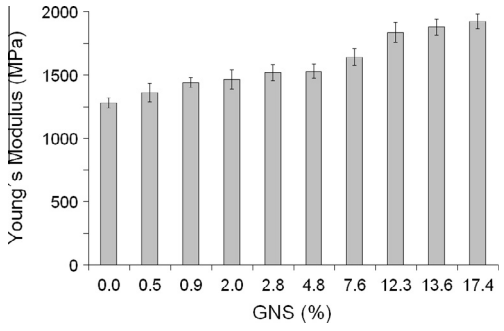

Fig. 4. Variation of Young's modulus with increasing GNS content in nanocomposites.

important above the glass transition temperature, i.e., when the polypropylene chain mobility is sufficiently high. From a practical point of view, these materials will show improved mechanical performance compared to the iPP with no variation in the final processing temperature (because T_m remains almost constant for all samples). This reinforcement effect is higher in the iPP materials prepared by *in situ* polymerization than in solution-blended nanocomposites [26].

Dynamic mechanical measurements provide information about the dimensional stability of different samples from the variation of displacement with temperature. Fig. 7 shows that deformability in pristine iPP (sample 1) is much higher than in the nanocomposite with 12.3% GNS (sample 8), and intermediate for the other specimens depending on the GNS content. These changes are more significant at temperatures above the glass transition temperature, as observed with the differences in rigidity of these samples.

For relaxation processes, the tan δ representations in the lower plot in Fig. 6 shows three main processes [27], labeled γ, β and α in order of increasing temperature. The γ mechanism overlaps the β process and has been attributed to local motions in the amorphous phase of iPP. The β relaxation is associated with generalized motion in the amorphous regions during the glass transition, while the transition at higher temperatures is attributed to the mobility within crystallites. The rigidity introduced by the presence of graphene slightly modifies the amorphous regions, and small differences are observed in the location and the intensity of the β process. Therefore, this β relaxation moves to slightly higher temperatures (10.0, 11.0, 11.5, 12.0 and 13.5 °C for neat iPP, iPP/GNS 0.9%, iPP/GNS 2.0%, iPP/GNS 4.8% and iPP/GNS 12.3%, respectively). Nevertheless, changes in the mobility within crystallites seem to be more important, and the α mechanism accordingly shifts to higher temperature (75.5, 81.0, 79.0, 82.0 and 82.0 °C for pristine iPP, iPP/GNS 0.9%, iPP/GNS 2.0%, iPP/GNS 4.8% and iPP/GNS 12.3%, respectively), and its intensity is reduced in nanocomposites relative to the iPP homopolymer.

3.8. Electrical conductivity

The values of the electrical conductivity of iPP and its nanocomposites are listed in Table 1. The conductivity of the neat iPP is virtually null (1.5×10^{-13} S cm^{-1}), as expected, which confirms the insulating nature of this material. Increasing the GNS content of

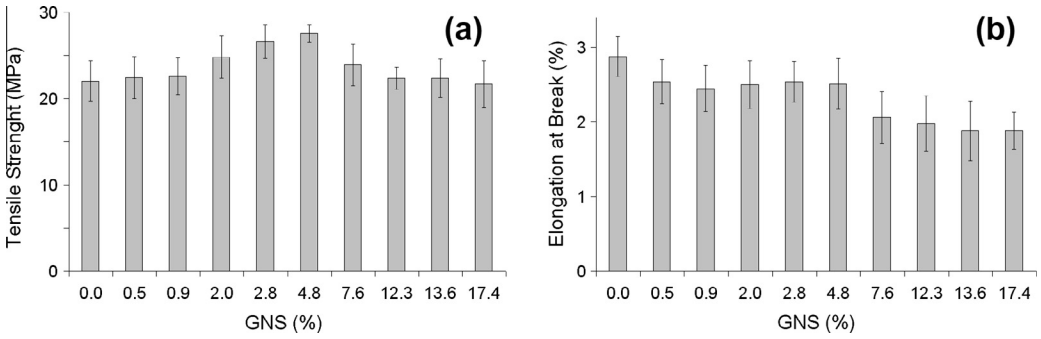

Fig. 5. Variation of the tensile strength (a) and the elongation at break (b) with increasing GNS content.

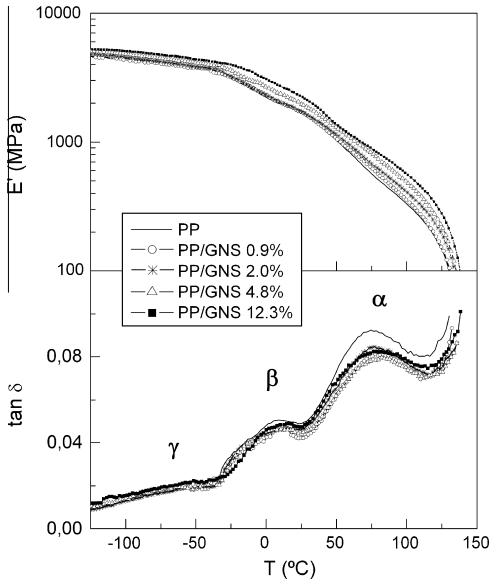

Fig. 6. Variation of the storage modulus and the loss tangent for different specimens.

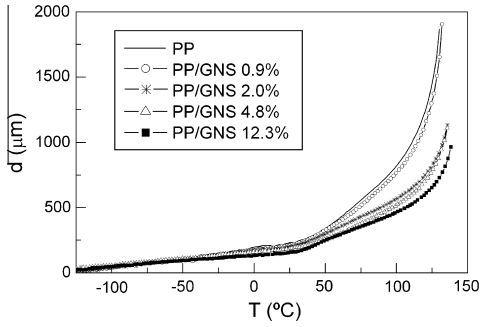

Fig. 7. Dimensional stability of iPP and iPP/GNS nanocomposites.

the nanocomposites produces an important increase in conductivity. Nanocomposites with a GNS content of 17.4 wt.% are more conductive than pristine iPP by a factor of 10^8. The conductivities obtained in this work are not as high as the values reported in other works [28,19]. A high degree of dispersion might not necessarily lead to higher conductivities. The SEM images showed that the graphene nanosheets were rather well wrapped up within the isolating iPP, which prevented direct inter-particle contact and decreased the conductivity [10]. In fact, a very low percolation thresholds have been achieved when the fillers were not homogeneously dispersed in the polymer matrix but rather segregated forming a conductive network [29].

4. Conclusions

Isotactic polypropylene/graphene nanosheet nanocomposites have been successfully synthesized by *in situ* polymerization using a metallocene catalyst. The molecular weight, polydispersity and tacticity of these nanocomposites are similar to those of neat iPP. The XRD profiles show almost complete exfoliation in the nanocomposites with the smallest graphene levels. The TEM images show good dispersion of GNS in the polymer matrix in nanocomposites with high GNS levels. Crystallization shifts to higher temperatures as GNS content increases because GNS functions as a nucleating agent. Nevertheless, the melting temperature and the crystallinity do not vary significantly in these nanocomposites because of the presence of GNS. The incorporation of GNS also improves the thermal stability and shifts the degradation temperature by more than 20 °C. Young's modulus increases continuously (50%), the tensile strength increases (25%), and the elongation at break decreases (30%) in these nanocomposites. Dynamic mechanical properties are consistent with the GNS reinforcement effect within iPP, which is more important above the glass transition temperature. Nanocomposites also exhibit superior dimensional stability relative to iPP. Finally, impedance measurements prove that the polymer conductivity increases by a factor of 10^8, and the iPP is transformed from an isolating polymer to a semiconductor. Although this increase in conductivity is high, only samples with more than 7.6 wt.% GNS show in the some conductivity, which was higher than other results reported in the literature. The *in situ* polymerization used to synthesize these nanocomposites most likely favors the growth of polymeric chains around GNS and facilitates their overall dispersion, hindering more efficient inter-particle contact.

Acknowledgments

The authors thank CAPES, FAPERGS-PRONEX, CNPq and the Department of the Navy Grant N62909-11-1-7069 issued by the Office of Naval Research Global for financial support. We also thank CNPq-PV for giving a grant to Prof. Raúl Quijada, and we thank Nacional de Grafite Ltda./Brazil for supplying the graphite Micrograf HC11.

References

[1] Alexandre M, Dubois P. Polymer-layered silicate nanocomposites: preparation, properties and uses of a new class of materials. Mat Sci Eng, R 2000;28:1–63.
[2] Garcés JM, Moll DJ, Bicerano J, Fibiger R, McLeod DG. Polymeric nanocomposites for automotive applications. Adv Mater 2000;12(23):1835–9.
[3] Moniruzzaman M, Winey KI. Polymer nanocomposites containing carbon nanotubes. Macromolecules 2006;39:5194–205.

[4] Alexandre M, Pluta M, Dubois P, Jérôme R. Metallocene catalyzed polymerization of ethylene in the presence of graphite. Macromol Chem Phys 2001;202:2239–46.
[5] Zheng G, Wu J, Wang W, Pan C. Characterizations of expanded graphite/polymer composites prepared by in situ polymerization. Carbon 2004;42:2839–47.
[6] Geim AK. Graphene: status and prospects. Science 2009;324:1530–4.
[7] Geim AK, Novoselov KS. The rise of graphene. Nat Mater 2007;6:183–91.
[8] Singh V, Joung D, Zhai L, Das S, Khondaker SI, Seal S. Graphene based materials: past, present and future. Prog Mater Sci 2011;56:1178–271.
[9] Fim FC, Guterres JM, Basso NRS, Galland GB. Polyethylene/graphite nanocomposites obtained by in situ polymerization. J Polym Sci, Part A: Polym Chem 2010;48:692–8.
[10] Potts JR, Dreyer DR, Bielawski CW, Ruoff RS. Graphene-based polymer nanocomposites. Polymer 2011;52:5–25.
[11] Pan YX, Yu ZZ, Ou YC, Hu GH. A new process of fabricating electrically conducting nylon 6/graphite nanocomposites via intercalation polymerization. J Polym Sci, Part B: Polym Phys 2000;38:1626–33.
[12] Chen G, Weng W, Wu D, Wu C. PMMA/graphite nanosheets composite and its conducting properties. Eur Polym J 2003;39:2329–35.
[13] Stankovich S, Dikin DA, Dommett GHB, Kohlhaas KM, Zimney EJ, Stach A, et al. Graphene-based composite materials. Nature 2006;442:282–6.
[14] Thostenson ET, Li C, Chou T. Nanocomposites in context. Compos Sci Technol 2005;65:491–516.
[15] Kim H, Abdala AA, Macosko CW. Graphene/polymer nanocomposites. Macromolecules 2010;43:6515–30.
[16] Gopakumar TG, Pagé DJYS. Polypropylene/graphite nanocomposites by thermo-kinetic mixing. Polym Eng Sci 2004;44:1162–9.
[17] Kalaitzidou K, Fukushima H, Drzal LT. Mechanical properties and morphological characterization of exfoliated graphite–polypropylene nanocompósitos. Composites Part A 2007;38:1675–82.
[18] Steurer P, Wissert R, Thomann R, Mülhaupt R. Functionalized graphenes and thermoplastic nanocomposites based upon expanded graphite oxide. Macromol Rapid Commun 2009;30:316–27.
[19] Wakabayashi K, Brunner PJ, Masuda J, Hewlett SA, Torkelson JM. Polypropylene–graphite nanocomposites made by solid-state shear pulverization: effects of significantly exfoliated, unmodified graphite content on physical, mechanical and electrical properties. Polymer 2010;51:5525–31.
[20] Song P, Cao Z, Cai Y, Zhao L, Fang Z, Fu S. Fabrication of exfoliated graphene-based polypropylene nanocomposites with enhanced mechanical and thermal properties. Polymer 2011;52:4001–10.
[21] Huang Y, Qin Y, Zhou Y, Niu H, Yu ZZ, Dong JY. Polypropylene/graphene oxide nanocomposites prepared by in situ ziegler–natta polymerization. Chem Mater 2010;22:4096–102.
[22] Huang Y, Qin Y, Wang N, Zhou Y, Niu H, Niu H, et al. Reduction of graphite oxide with a grignard reagent for facile in situ preparation of electrically conductive polyolefin/graphene nanocomposites. Macromol Chem Phys 2012;213:720–8.
[23] Polschikov SV, Nedorezova PM, Klyamkina AN, Kovalchuk AA, Aladyshev AM, Shchegolikhin AN, et al. Composite materials of graphene nanoplatelets and polypropylene, prepared by in situ polymerization. J Appl Polym Sci 2012. http://dx.doi.org/10.1002/APP.37837.
[24] Milani MA, Quijada R, Basso NRS, Graebin AP, Galland GB. Influence of the graphite type on the synthesis of polypropylene/graphene nanocomposites. J Polym Sci, Part A: Polym Chem 2012;50:3598–605.
[25] Rodrigues IR, Forte MMC, Azambuja DS, Castagno KRL. Synthesis and characterization of hybrid polymeric networks (HPN) based on polyvinyl alcohol/chitosan. React Funct Polym 2007;67:708–15.
[26] Wang Y, Tsai HB. Thermal, dynamic-mechanical, and dielectric properties of surfactant intercalated graphite oxide filled maleated polypropylene nanocomposites. J Appl Polym Sci 2012;123:3154–63.
[27] Jourdan C, Cavaille JY, Perez J. Mechanical relaxations in polypropylene: a new experimental and theoretical approach. J Polym Sci, Part B: Polym Phys 1989;27:2361–84.
[28] Kalaitzidou K, Fukushima H, Drzal LT. A new compounding method for exfoliated graphite–polypropylene nanocomposites with enhanced flexural properties and lower percolation threshold. Compos Sci Technol 2007;67:2045–51.
[29] Pang H, Chen T, Zhang G, Zeng B, Li ZM. An electrically conducting polymer/graphene composite with a very low percolation threshold. Mater Lett 2010;64:2226–9.